Research Paper

Vibrational Properties of Quinones in the A_1 Binding Site of Photosystem I Calculated Using a Three-Layer ONIOM Method

Leyla Rohani and Gary Hastings*

Department of Physics and Astronomy, Georgia State University, Atlanta, Georgia 30302, USA.
**Corresponding author, Gary Hastings, Email: ghastings@gsu.edu*

Received 30 April, 2019, revised 24 May 2019, accepted 25 May 2019
Publication Date (Web): May 25, 2019

Abstract

A three-layer ONIOM method (QM-high:QM-low:MM) has been used to calculate the vibrational properties of neutral and reduced 2-methyl-3-phytyl-1,4-naphthoquinone (phylloquinone (PhQ)) and 2-methyl-1,4-naphthoquinone (2MNQ) in the A_1 binding site of photosystem I (PSI). Calculated spectra for both the neutral and reduced quinones are compared to FTIR difference spectra. For the reduced quinones, the calculated and experimental spectra agree well. In a previous study that utilized a three-layer ONIOM method, the calculated spectra for the reduced quinones did not agree well with experimental spectra (Makita et, al. 2017). The improvement in this study is that we have extended the size of the molecular model used in calculations to include several (six) water molecules that are in the vicinity of the quinones in the A_1 binding site. With this molecular model good agreement with experiment is obtained. The inclusion of water molecules in the molecular model improves the agreement between calculated and experimental spectra for both semiquinones. However, a lack of solid experimental data for the neutral quinones precludes a similar comparison. So the calculated spectra for neutral quinones presented here is a prediction that awaits experimental verification.

Keywords

Photosystem I, A_1, Phylloquinone, FTIR difference spectroscopy, Three-layer ONIOM calculation, QM-high/QM-low/MM method, Density functional theory.

Introduction

In photosystem I (PSI) photosynthetic reaction centers light induces the transfer of electrons via a series of acceptors across a biological membrane (Golbeck and Bryant 1991, Golbeck 2006). One of the intermediates in the electron transfer chain is a protein bound phylloquinone (PhQ) molecule that occupies the so-called A_1 binding site (Brettel 1997). X-ray structures from different strains indicate very similar structural details for PhQ in the A_1 binding site and surrounding amino acids (Jordan et, al. 2001, Mazor et, al. 2014, Mazor et, al. 2017). These crystal structures show that PhQ is asymmetrically hydrogen bonded (H-bonded), with the C_1=O group being free

from H-bonding while the C_4=O group is H-bonded to the backbone nitrogen atom of a leucine residue (Figure 1A). In attempts to model this asymmetric H-bonding, gas phase calculations for PhQ in the presence of an H-bonding water molecule or truncated leucine residues have been undertaken (Bandaranayake et, al. 2006, Makita and Hastings 2018). These simple H-bonded PhQ models allowed a first interpretation of FTIR experimental spectra. However, these models do not account for contributions from the charged environment near PhQ. Such local charges are important for reproducing experimental data (Thompson et, al. 2014).

It is now well established that in PSI complexes isolated from *men*B$^-$ mutant cells, non-native quinones can be incorporated into the A_1 binding site (Johnson et, al. 2000) and time-resolved FTIR difference spectroscopy (DS) has been used to study PSI particles with many different quinones incorporated (Makita et, al. 2015, Makita and Hastings 2018). The goal of the work presented here is to develop a computational method to simultaneously simulate FTIR DS obtained for PSI with many different quinones incorporated.

Despite software developments and the availability of high-performance computers, it is still challenging to calculate properties of a large molecular system using quantum mechanical (QM) methods (Chung et, al. 2015). One solution to this problem is to consider a small portion of a larger molecular structure at a QM level of theory, while treating the rest of the molecular structure at a lower level of theory (Svensson et, al. 1996, Vreven et, al. 2003). One can even parse the molecular system further by considering a three-layer system where the pigment of interest is treated at a high QM level of theory, interacting amino acids are considered at a lower QM level of theory, and more distant atoms are treated at a molecular mechanics (MM) level of theory (Svensson et al. 1996, Hall et, al. 2008, Chung et al. 2015). The three-layer approach is implemented in Gaussian16 software (Frisch et al. 2016), using ONIOM (Frisch et, al. 2016). ONIOM is an acronym for: our Own N-layered Integrated molecular Orbital and molecular Mechanics model (Svensson et al. 1996, Chung et al. 2015). Such a three-layer approach offers some desirable advantages. For example, a three-layer ONIOM method allows the calculation of normal-mode potential energy distributions (PEDs) for the bound quinones. This in turn allows a more quantitative interpretation and assessment of bands in the experimental spectra (Makita et al. 2017, Rohani and Hastings 2018).

Previously, we attempted to simulate FTIR DS for PSI with PhQ and 2MNQ incorporated into the A_1 binding site using a three-layer ONIOM model (Makita et al. 2017). Spectra calculated using this model, however, did not simulate well the experimental spectra for reduced states of both quinones (semiquinones) in the A_1 binding site. Progressing from this previous study, here we consider a more extensive molecular model that now includes several water molecules in the QM-low layer. The newly included water molecules are likely important as they are conserved in all of the available crystal structures. We show here that their inclusion leads to an improved simulation of experimental FTIR DS.

Materials and Methods

The molecular model was constructed using the x-ray structure of cyanobacterial PSI at 2.5 Å resolution (PDB entry 1JB0) (Jordan et al. 2001). The model consists of atoms that are within 12 Å of either carbonyl oxygen atom of PhQ (Figure 1A).

The phytyl tail of PhQ was truncated to a 5-carbon unit [$CH_2CHC(CH_3)_2$]. Hydrogen atoms were added to the molecular model using GaussView6 (Frisch et al. 2016). Standard protonation states were used for all amino acids. All heavy atoms of amino acid residues were constrained. Oxygen of water molecules, heavy atoms of quinone, as well as all hydrogen atoms, were unconstrained. We have shown previously that the calculated results do not depend much on whether amino acids' side chains were constrained or unconstrained (Makita et al. 2017).

The QM-high layer, includes only atoms of the bound quinone (Figure 1A). The QM-high calculations were undertaken using hybrid DFT methods, employing the B3LYP functional and the 6-31+G(d) basis set. It was shown that this combination is appropriate for calculations of semiquinones (Bandaranayake et, al. 2006). The QM-low layer consists of LeuA722; TrpA697; PheA689; SerA692, and MetA688; part of AlaA721, SerA723, IleA724; and six water molecules (Figure 1A). The QM-low layer is treated using B3LYP functional and the 6-31G(d) basis set. A similar selection of residues, without inclusion of water molecules, was considered

previously (Makita et al. 2017, Rohani and Hastings 2018).

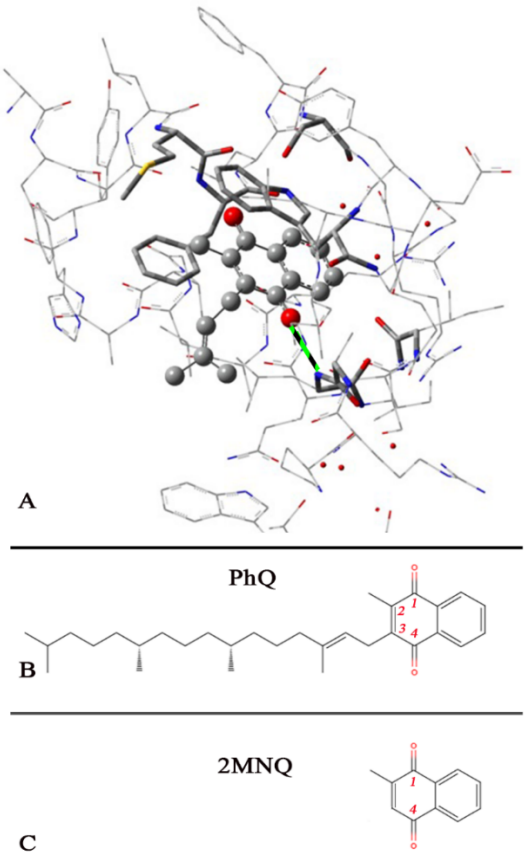

Figure 1: (A) Model used in three-layer ONIOM calculations. Quinone atoms are treated at the QM-high level and are shown as ball and bond. The nearby environment of PhQ is at the QM-low level and is shown as tubes. The remainder of the atoms are treated at the MM level and are shown as thin sticks. H-bond is shown in green. Hydrogen atoms are not shown. Six water molecules are modeled at the QM-low level (red). Structure and numbering of (B) PhQ, and (C) 2MNQ.

The third layer consists of atoms of all remaining residues (Figure 1A), and is treated at the MM level of theory using UFF (Rappe et, al. 1992). The QM-low layer was connected to the MM layer using the link atom approach (Chung et al. 2015).

For modeling 2MNQ in the A_1 binding site, the truncated tail of PhQ is replaced by a hydrogen atom (Figure 1C). Only the specific orientation of 2MNQ with the methyl group meta to the H-bond was chosen, as this appears to be the orientation adopted in PSI (Pushkar et, al. 2002, van der Est et, al. 2010, Makita et al. 2017). The structure and numbering of PhQ/2MNQ is shown in Figure 1B/C, respectively.

In the designed three-layer ONIOM model, the QM-high layer consists of quinone. While the negative charge should be considered over the quinone to model the reduced state (the negative charge affects the quinonic ring and two carbonyl groups mainly). The QM-low layer highly interacts with the QM-high layer also. Indeed for modeling one-electron reduced state at the QM-high layer using the three-layer ONIOM methods, two choices have been suggested (Hall et al. 2008). In the first option, the QM-low and QM-high layers might have the same negative charge assignment (Hall et al. 2008). In the second option, the QM-high layer might be included no charges, whereas the QM-low layer includes a negative charge assignment (Hall et al. 2008). In the second choice, the negative charge has been accurately included in the calculations at the QM-high layer (Hall et al. 2008).

In this research, we selected the first choice, whereas the calculated spectrum based on two options are the same (not presented here). It is noticeable that if we select a charge of -1 at the QM-high layer and a charge of zero at the QM-low layer, calculated vibrational frequencies do not simulate the semiquinone properties (not presented here). Based on the protonation of residues in the entire molecular structure and overall charge of the amino acids in the structure, the MM layer charge assignment is set to be equal to +1.

Following geometry optimization of the quinones in the binding site, the optimized quinones were extracted and considered separately for normal mode vibrational frequency calculations. This approach was employed successfully for previous two-layer (Lamichhane and Hastings 2011) and three-layer (Makita et al. 2017) ONIOM calculations.

Although atomic displacements can be animated using GaussView6 software, and the most prominent contribution to the normal modes can be assessed visually, calculated potential energy distributions (PEDs) allow a more quantitative assessment of the contribution of different molecular groups to the normal modes. PEDs were calculated using VEDA (Jamroz 2013).

Results and Discussion

Previously we have established that PhQ^- gives rise to bands at 1494 and 1414 cm^{-1} in time-resolved

FTIR DS (Sivakumar et, al. 2005, Hastings et, al. 2008) (Hastings 2015, Makita et al. 2017). Only two intense vibrational frequencies were calculated for PhQ^- also. Consequently, the two intense calculated vibrations of PhQ^- were shifted to the observed frequencies. A 0.9739 factor from 1600 to 1420 cm^{-1}, and a 0.9965 factor from 1460 to 1390 cm^{-1} scaled the calculated anion frequencies. Two individual shifted spectra were merged to produce the calculated scaled anion spectrum (1600 -1390 cm^{-1}) at the next step. For the neutral PhQ, no band has been confirmed by the experimental data, so, we scaled the neutral spectrum undertaking an arbitrary factor (0.9662). Calculated frequencies (scaled) and mode assignments are listed in Table 1.

Scaled calculated spectra for both the neutral and reduced quinone states were then used to produce a calculated "reduced minus neutral" FTIR DS for PhQ (Figure 2a) and 2MNQ (Figure 2b). The corresponding FTIR DS are also shown in Figure 2 (*dotted*). By subtracting the FTIR DS obtained for PhQ from that obtained from 2MNQ, a (2MNQ – PhQ) double difference spectrum (DDS) is constructed (Figure 2*c*). DDS are useful as common protein bands can cancel, allowing one to distinguish quinone from protein bands. The corresponding FTIR DDS is also shown in Figure 2d. The standard error in multiple repeated experiments is shown shaded in Figure 1d.

Neutral quinones display intense absorption due to C=O and C=C vibrations in the ~1670-1580 cm^{-1} region (Breton et, al. 1994). Semiquinones display absorption at lower frequencies, in the ~1550-1400 cm^{-1} spectral region (Breton et al. 1994). Below we will discuss the anion and neutral bands in each spectral region separately.

Neutral Bands

Calculations for neutral PhQ indicate an intense band at 1658 cm^{-1} (Figure 2a) which is due to the C_1=O stretching vibration (82%) (Table 1). The corresponding mode for neutral 2MNQ is calculated 10 cm^{-1} higher, at 1668 cm^{-1} (80%) (Table 1). The calculated frequencies for the C_1=O vibration for the neutral quinones agree with previous calculations (Makita et al. 2017), and the extended QM layer considered here did not change this result.

The C_1=O vibration gives rise to a difference band at 1658(+)/1668(–) cm^{-1} in the calculated DDS (Figure 2c). However, such a difference band is not observed in the experimental FTIR DDS. At present it is unclear if the lack of observation of a clear C_1=O difference feature in the experimental DDS is due to PhQ and 2MNQ in PSI having a C_1=O mode at similar frequency, and/or whether a difference feature is masked because of inadequate signal to noise levels in the experimental spectra.

For both neutral quinones the C_4=O group is calculated to contribute significantly to several normal modes (Table 1). The most obvious feature in the calculated DDS in Figure 2c is the 1610(+)/1633(–) difference band, and this feature is calculated to be due to, at least in part, a C_4=O vibration. However, the calculated difference feature has an even greater contribution from the C_2=C_3 stretching vibration (39-40%) (Table 1).

The calculated DDS in the neutral region (~1670-1580 cm^{-1}) in Figure 2c differs from the DDS calculated in previous three-layer ONIOM calculation using a simpler molecular model (see Figure 4 and S5 in (Makita et al. 2017)). The differences in the DDS in the two studies arise mainly because of differences in calculated frequencies and mode compositions associated with the C_4=O group. So the inclusion of water molecules near the quinone has quite a profound influence on the calculated molecular modes of the incorporated (neutral) quinones. Such a conclusion is of some importance, as it sheds some light on what should be included in molecular models being used for future ONIOM calculations.

As found above for the C_1=O DDS feature, the calculated 1610(+)/1633((–) difference feature in the DDS appears not to be obvious in the experimental FTIR DDS. Again, this could be partly due to limitations in the signal to noise ratio in the experiment.

Anion Bands

For PhQ^- in the A_1 binding site, an intense band is calculated at 1494 cm^{-1} (Figure 2a). The PED calculations show this band is due mainly to the $C_1 \cdots O$ stretching vibration (43%) (Table 1). The corresponding mode for $2MNQ^-$ is calculated 13 cm^{-1} higher, at 1507 cm^{-1} (51%). These modes give rise to the 1507(+)/1494(−) cm^{-1} feature in the calculated DDS (Figure 2c). Although the composition of the calculated normal modes is slightly altered, similar mode assignments were suggested previously (Makita et al. 2017). In addition, the calculated DDS feature is in good agreement with experiment (compare Figure 1c and d).

Table 1: Calculated normal modes (in cm^{-1}) and intensities (in km/mol) for neutral and reduced PhQ and 2MNQ in the A_1 binding site. The neutral frequencies are scaled by 0.9662. In the anion region two scaling factors are used (0.9739 so that the intense calculated and experimental bands match near 1495 cm^{-1}, and 0.9965 so that intense calculated and experimental bands match near 1415 cm^{-1}). Experimental bands are indicated in italics. Mode assignments and calculated PEDs (in parenthesis, in %) are indicated. Abbreviations: *v*, stretching; δ, bending; a, aromatic ring.

PhQ	**Int.**	**PED**	**2MNQ**	**Int.**	**PED**
1658	200.2	$\nu(C_1{=}O)$ (82)	1668	174.7	$\nu(C_1{=}O)$ (80)
1610	63.8	$\nu(C_4{=}O)$ (17) + $\nu(C_2{=}C_3)$ (39)	1633	129.0	$\nu(C_2{=}C_3)$ (38) + $\nu(C_4{=}O)$ (20)
1597	60.0	$\nu(C_4{=}O)$ (40) + $\nu(C_2{=}C_3)$ (26)	1594	39.8	$\nu(C_2{=}C_3)$ (19) + $\nu(C{-}C)_a$ (19) + $\nu(C_4{=}O)$ (20)
1578	103.9	$\nu(C_4{=}O)$ (12) + $\nu(C_2{=}C_3)$ (26) + $\nu(C{-}C)_a$ (23)	1576	120.9	$\nu(C{-}C)_a$ (51) + $\nu(C_4{=}O)$ (13)
1564	39.8	$\nu(C_4{=}O)$ (17) + $\nu(C{-}C)_a$ (36)	1561	61.5	$\nu(C{-}C)_a$ (36) + $\nu(C_4{=}O)$ (20)
1561	61.5	$\nu(C{-}C)_a$ (36) + $\nu(C_4{=}O)$ (20)			
PhQ^-	**Int.**	**PED**	**$2MNQ^-$**	**Int.**	**PED**
1520	56.2	$\nu(C_1{=}O)$ (14) + $\nu(C_2{=}C_3)$ (14) + $(C\text{-}C)_a$ (12)	1532	27.1	$\nu(C_2{=}C_3)$ (15)
1494 (*1494*)	215.2	$\nu(C_1{=}O)$ (43) + $\nu(C_2{=}C_3)$ (18)	1507 (*1505*)	296.8	$\nu(C_1{=}O)$ (51)+ $\nu(C_1{-}C_2)$ (10)
1435	30.4	$\nu(C_4{=}O)$ (23)			
1415 (*1415*)	186.7	$\nu(C_4{=}O)$ (24) + $\nu(C_4{-}C_3)$ (15) + $\delta(CCH)_a$ (11)	1433 (*1429*)	159.5	$\nu(C_4{=}O)$ (45)
1404	44.1	$\delta(C_{methyl}H_2)$ (41)			

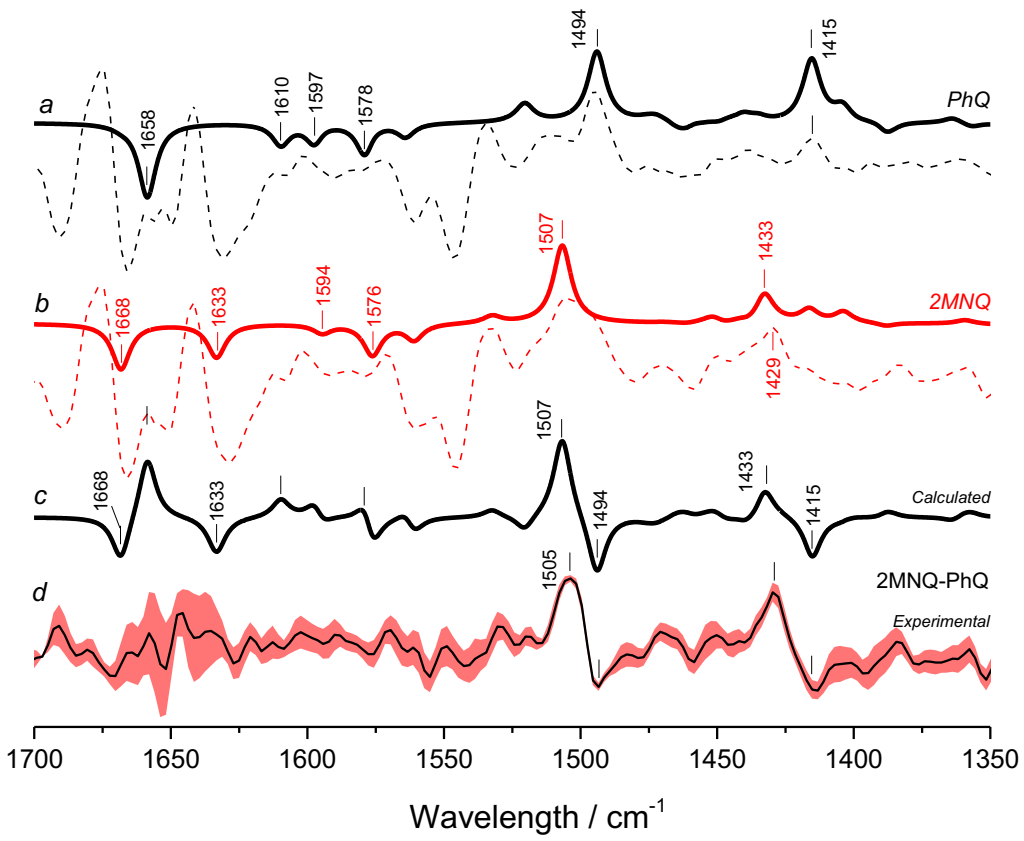

Figure 2: Calculated "reduced minus neutral" DS for PhQ (*a*, black) and 2MNQ (*b*, red) in the A_1 binding site. Corresponding experimental ($A_1^- - A_1$) FTIR DS are also shown (*dotted*). Calculated (c) and experimental (d) (2MNQ – PhQ) DDS obtained by subtracting the spectra in (*a*) from that in (*b*). Shading in (*d*) is the standard error obtained from repeated measurements. Frequencies calculated for neutral quinones are scaled by 0.9662. Frequencies calculated for semiquinones are scaled by 0.9739 and 0.9965. Further TR FTIR DS experiments on PSI with PhQ and 2MNQ incorporated have been undertaken recently, and the experimental spectra shown here are updated versions from that shown previously (Makita et al. 2017) .

For PhQ^-, the calculated normal mode at 1415 cm^{-1} contains a 24% contribution from the $C_4{=}O$ stretching vibration, and also contributions from other molecular groups (Table 1). The corresponding mode for $2MNQ^-$ is calculated at 1433 cm^{-1} where the $C_4{=}O$ vibration contributes ~45% to the normal mode (Table 1). These modes give rise to the 1433(+)/1415(−) cm^{-1} feature in the calculated DDS (Figure 2c). Although the composition of the calculated normal modes were very different, a similar DDS feature was also calculated previously (Makita et al. 2017).

In the anion region (~1550-1400 cm^{-1}), the calculated and experimental DDS are in excellent agreement (compare Figure 2*c* and 2*d*). However, in the previous work, the predominantly $C_4{=}O$ vibration of both $2MNQ^-$ and PhQ^- were calculated at 1426 cm^{-1} with the mode of $2MNQ^-$ having greater than double the intensity of the corresponding mode of PhQ^- (Makita et al. 2017). Calculations undertaken using the simpler molecular model (without water molecules) did not simulate the tangible band-shift from 1429 to 1415 cm^{-1} (~14 cm^{-1}) of the experimental data. Therefore, based on the simpler model (with 100% error), it was difficult to rationalize the result, as pointed out previously (Makita et al. 2017).

The current model suggests ~18 cm^{-1} upshifting for the replacement of 2MNQ in the molecular model (28.5% error). Consequently, the current simulated band-shift is considered as an improvement respecting to the former. It should be noted that the band-shift in DDS due to the replacement of the quinones in the molecular structure is independent of the scaling factors, whereas multiple scaling factors make the straightforward comparison between the calculated and FTIR DDS.

So, although the two calculations yield somewhat similar spectral profiles, the calculations using the current molecular model predict very different mode frequencies and intensities. Mode frequencies and intensities that are in line with experiment, however. The present calculations are clearly an improvement over previous calculations in this respect.

The calculations reported here indicate that the semiquinone C⋯O modes are separated by 74-79 cm^{-1}. Such a large downshift could suggest a very strong H-bonding to the semiquinone C_4⋯O group. Such asymmetric H-bonding to the quinone in the A_1 binding site has been reviewed previously (Srinivasan and Golbeck 2009). Such highly asymmetric H-bonding is unlike that found for quinones in the Q_A binding site in purple bacterial reaction centers (Breton and Nabedryk 1996) and in photosystem II (PSII) (Noguchi et, al. 1999).

It was suggested that the presence of water molecules near the H-bonded carbonyl group of the quinone in the A_1 binding site might have an impact on the strength of the H-bond (Pushkar et, al. 2004). We show here that such water molecules impact the normal modes, and hence electronic structure of the bound quinone, and molecular interactions with water molecules are necessary to adequately simulate the experimental spectra. However, calculations using molecular models without these additional water molecules might also predict a strong asymmetric H-bonding. So it is unclear exactly how or if these water molecules contribute to strong H-bonding. What is clear is that molecular interactions with water molecules are necessary to adequately simulate the experimental FTIR DDS.

Here we show that the inclusion of water molecules in the QM-low layer of a three-layer ONIOM calculation leads to better agreement between calculated and experimental DDS (Figure 2c /2d). The inclusion of six water molecules (18 atoms) in the QM-low layer considerably increases the computational effort required in the geometry optimization step. So one goal for future work could be to include the water molecules in the QM-low layer but decrease the size of the QM-low layer by establishing which amino acids can be removed without undue influence on the calculated spectra.

Conclusions

We optimized the geometry of PhQ and 2MNQ in the A_1 binding site using a three-layer ONIOM method. This method allows the calculation of PEDs, which gives quantitative insight into normal mode composition.

In comparison to our previous molecular models, the size of the molecular model considered here was extended to include six water molecules, that were included in the QM-low layer. Our calculations indicate that the inclusion of water molecules has a significant impact on the H-bonded carbonyl vibration modes of both the neutral and reduced quinones. In contrast, the vibrational properties of the non-H-bonded carbonyl groups of both quinones did not change dramatically.

Acknowledgements

This material is based upon work supported by the U.S. Department of Energy, Office of Science, Office of Basic Energy Sciences, under Award Number DE-SC-0017937 to GH. We acknowledge the use of Georgia State research computing resources that are supported by Georgia State Research Solutions.

References

Bandaranayake, K., et al. (2006). "Modeling The A_1 Binding Site In Photosystem I. Density Functional Theory For The Calculation Of "Anion – Neutral" FTIR Difference Spectra of Phylloquinone." Vibrational Spectroscopy **42**(1): 78-87.

Bandaranayake, K. M. P., et al. (2006). "Modification of the phylloquinone in the A(1) binding site in photosystem I studied using time-resolved FTIR difference spectroscopy and density functional theory." Biochemistry **45**(13): 4121-4127.

Breton, J., et al. (1994). "The binding sites of quinones in photosynthetic bacterial reaction centers investigated by light-induced FTIR difference spectroscopy: assignment of the Q_A vibrations in R*hodobacter sphaeroides* using ^{18}O- or ^{13}C-labeled ubiquinone and vitamin K_1." Biochemistry **33**(16): 4953-4965.

Breton, J. and Nabedryk, E. (1996). "Protein-quinone interactions in the bacterial photosynthetic reaction center: light-induced FTIR difference spectroscopy of the quinone vibrations." Biochimica et Biophysica Acta (BBA) - Bioenergetics **1275**(1): 84-90.

Brettel, K. (1997). "Electron transfer and arrangement of the redox cofactors in photosystem I." Biochimica et Biophysica Acta (BBA) - Bioenergetics **1318**(3): 322-373.

Chung, L. W., et al. (2015). "The ONIOM Method and Its Applications." Chemical Reviews **115**(12): 5678-5796.

Frisch, M. J., et al. (2016). Gaussian 16 Rev. B.01. Wallingford, CT.

Golbeck, J. (2006). Photosystem I The Light Driven Plastocyanin:Ferridoxin Oxidoreductase. Dordrecht, Springer.

Golbeck, J. H. and Bryant, D. (1991). Photosystem I. Current topics in bioenergetics. New York, Academic Press. **16:** 83-175.

Hall, K. F., et al. (2008). "Three-Layer ONIOM Studies of the Dark State of Rhodopsin: The Protonation State of Glu181." Journal of Molecular Biology **383**(1): 106-121.

Hastings, G. (2015). "Vibrational spectroscopy of photosystem I." Biochimica et Biophysica Acta (BBA) - Bioenergetics **1847**(1): 55-68.

Hastings, G., et al. (2008). "Time-resolved FTIR difference spectroscopy in combination with specific isotope labeling for the study of A(1), the secondary electron acceptor in photosystem 1." Biophysical Journal **94**(11): 4383-4392.

Jamroz, M. H. (2013). "Vibrational energy distribution analysis (VEDA): scopes and limitations." Spectrochimica Acta Part A: Molecular and Biomolecular Spectroscopy **114**: 220-230.

Johnson, T. W., et al. (2000). "Recruitment of a foreign quinone into the A(1) site of photosystem I. I. Genetic and physiological characterization of phylloquinone biosynthetic pathway mutants in Synechocystis sp. pcc 6803." Jornal of Biological Chemistry **275**(12): 8523-8530.

Jordan, P., et al. (2001). "Three-dimensional structure of cyanobacterial photosystem I at 2.5 angstrom resolution." Nature **411**(6840): 909-917.

Lamichhane, H. P. and Hastings, G. (2011). "Calculated vibrational properties of pigments in protein binding sites." Proc Natl Acad Sci U S A **108**(26): 10526-10531.

Makita, H. and Hastings, G. (2018). "Photosystem I with benzoquinone analogues incorporated into the A_1 binding site." Photosynth Research **137**(1): 85-93.

Makita, H. and Hastings, G. (2018). "Time-resolved step-scan FTIR difference spectroscopy for the study of photosystem I with different benzoquinones incorporated into the A_1 binding site." Biochimica et Biophysica Acta (BBA) - Bioenergetics **1859**(11): 1199-1206.

Makita, H., et al. (2017). "Quinones in the A_1 binding site in photosystem I studied using time-resolved FTIR difference spectroscopy." Biochimica et Biophysica Acta (BBA) - Bioenergetics **1858**(9): 804-813.

Makita, H., et al. (2015). "Time-resolved visible and infrared difference spectroscopy for the study of photosystem I with different quinones incorporated into the A_1 binding site." Biochimica et Biophysica Acta (BBA) - Bioenergetics **1847**(3): 343-354.

Mazor, Y., et al. (2017). "Structure of the plant photosystem I supercomplex at 2.6 angstrom resolution." Nature Plants **3**(3).

Mazor, Y., et al. (2014). "Crystal structures of virus-like photosystem I complexes from the mesophilic cyanobacterium Synechocystis PCC 6803." Elife **3**.

Noguchi, T., et al. (1999). "Hydrogen bonding interaction between the primary quinone acceptor Q(A) and a histidine side chain in photosystem II as revealed by Fourier transform infrared spectroscopy." Biochemistry **38**(1): 399-403.

Pushkar, Y. N., et al. (2004). "Asymmetric Hydrogen-Bonding of the Quinone Cofactor in Photosystem I Probed by 13C-Labeled Naphthoquinones." The Journal of Physical Chemistry B.

Pushkar, Y. N., et al. (2002). "Orientation and Protein-Cofactor Interactions of Monosubstituted n-Alkyl Naphthoquinones in the A_1 Binding Site of Photosystem I." The Journal of Physical Chemistry B **106**: 12052-12058.

Rappe, A. K., et al. (1992). "Uff, a Full Periodic-Table Force-Field for Molecular Mechanics and

Molecular-Dynamics Simulations." Journal of the American Chemical Society **114**(25): 10024-10035.

Rohani, L. and Hastings, G. (2018). "Vibrational Frequency Calculations of Phylloquinone in the A_1 binding site: Layer Selection in ONIOM Methods." Frontiers in Science, Technology, Engineering and Mathematics **2**(3): 130-137.

Sivakumar, V., et al. (2005). "A(1) reduction in intact cyanobacterial photosystem I particles studied by time-resolved step-scan Fourier transform infrared difference spectroscopy and isotope labeling." Biochemistry **44**(6): 1880-1893.

Srinivasan, N. and Golbeck, J. H. (2009). "Protein–cofactor interactions in bioenergetic complexes: The role of the A_1A and A_1B phylloquinones in Photosystem I." Biochimica et Biophysica Acta (BBA) - Bioenergetics **1787**(9): 1057-1088.

Svensson, M., et al. (1996). "ONIOM: A Multilayered Integrated MO + MM Method for Geometry Optimizations and Single Point Energy Predictions. A Test for Diels−Alder Reactions and Pt(P(t-Bu)3)2 + H2 Oxidative Addition." The Journal of Physical Chemistry **100**(50): 19357-19363.

Thompson, L. M., et al. (2014). "Analytical Harmonic Vibrational Frequencies for the Green Fluorescent Protein Computed with ONIOM: Chromophore Mode Character and Its Response to Environment." Jornal of Chemical Theory and Computation **10**(2): 751-766.

van der Est, A., et al. (2010). "Incorporation of 2,3-Disubstituted-1,4-Naphthoquinones into the A_1 Binding Site of Photosystem I Studied by EPR and ENDOR Spectroscopy." Applied Magnetic Resonance **37**(1-4): 65-83.

Vreven, T., et al. (2003). "Geometry optimization with QM/MM, ONIOM, and other combined methods. I. Microiterations and constraints." Journal of Computational Chemistry **24**(6): 760-769.

Citation:
Leyla Rohani, Gary Hastings (2019). Vibrational Properties of Quinones in the A_1 Binding Site of Photosystem I Calculated Using a Three-Layer ONIOM Method, *Frontiers in Science, Technology, Engineering and Mathematics*, **Volume 3**, Issue 2, 91-99
